Int. J. Electrochem. Sci., 9 **(2014)** 3246 - 3258

International Journal of
ELECTROCHEMICAL
SCIENCE
www.electrochemsci.org

Effect of Electrochemical Potential and Chloride Concentration on Stress Corrosion Cracking Behavior of 23Co14Ni12Cr3Mo Ultra-High Strength Steel in NaCl Solution

Jianhua Liu[*]*, Kuo Zhao, Mei Yu, Songmei Li, Chen Wen*

School of Materials Science and Engineering, Beihang University, Beijing, 100191, China
E-mail: liujh@buaa.edu.cn

Received: 18 January 2014 / *Accepted:* 25 February 2014 / *Published:* 23 March 2014

The effect of electrochemical potential and chloride concentration on stress corrosion cracking (SCC) behavior of 23Co14Ni12Cr3Mo ultra-High strength steel were investigated by using slow strain rate technique (SSRT). Microstructure or morphology of fracture surfaces are characterized by using SEM at different applied potential conditions and NaCl concentrations. The SCC is attributed to the anodic dissolution at the open circuit potential (OCP), which is affected with Cl^- ions' existence. The SCC mechanism is anodic dissolution based, combined with hydrogen induced cracking. At applied potentials range from -550 to -395mV$_{SCE}$, i.e. -500mV$_{SCE}$, the 23Co14Ni12Cr3Mo steel is under cathodic protection, and the fracture morphologies are dimpled pattern dominated. Both positive and negative potential shift increase the SCC susceptibility of 23Co14Ni12Cr3Mo steel.

Keywords: 23Co14Ni12Cr3Mo, ultra-high strength steel, HE, slow strain rate test

1. INTRODUCTION

Ultra-high strength steels are usually developed for high performance with high strength and fracture toughness. As a crucial mode of material failures in corrosive environment, SCC remains one of the most serious limitations for the use of ultra-high strength steels [1-4].With excellent properties combined strength and ductility, the secondary hardening type of ultra-high strength steel 23Co14Ni12Cr3Mo is susceptible to SCC [5-6].

The SCC behavior of a material in application can be influenced by many factors [7~8], such as stress, anion ions, electrochemical properties, pH, humidity, and temperature [9~11]. Electrochemical properties and chloride ion are the two main factors which affected the corrosion behaviors of Ultra-high strength steels servicing in marine environments [8, 12~14].

In previous work, Many efforts have been done to study the corrosion behavior of 23Co14Ni12Cr3Mo steel [15~17]. The SCC susceptibility was investigated by constant load method (CL) with different load levels and slow strain rate technique (SSRT) with different strain rate, which demonstrated that the SCC regions can be divided into three regions as stress-dominated region, SCC-dominated region, and corrosion-dominated region, respectively. In this work, the effect of electrochemical potential and chloride concentration on the SCC behavior of 23Co14Ni12Cr3Mo steel in NaCl Solution has been studied by SSRT and electrochemical measurements, and the mechanism were characterized by fracture morphology.

2. EXPERIMENTAL

2.1 Material and microstructure

The chemical composition of 23Co14Ni12Cr3Mo steel is listed in Table1. Specimens were cut from a forged and annealed bar, which was heat treated as follows: solution treated in vacuum at 885°C vacuum for 1h, air cooled to room temperature for 2h, chilled at -73°C for 1h, and tempered at 482 °C for 5h. As the result, the σ_b and $\sigma_{0.2}$ of 23Co14Ni12Cr3Mo steel are 1960 MPa and 1690 MPa, respectively. Fig.1 shows the microstructure of 23Co14Ni12Cr3Mo steel. The result demonstrates that the 23Co14Ni12Cr3Mo steel mainly consists of lath/plant martensite and few reverted austenite.

Table 1. Chemical composition of 23Co14Ni12Cr3Mo steel, wt.%

Material	C	Co	Ni	Cr	Mo	Fe
23Co14Ni12Cr3Mo	0.23	13.4	11.1	3.1	1.2	Bal.

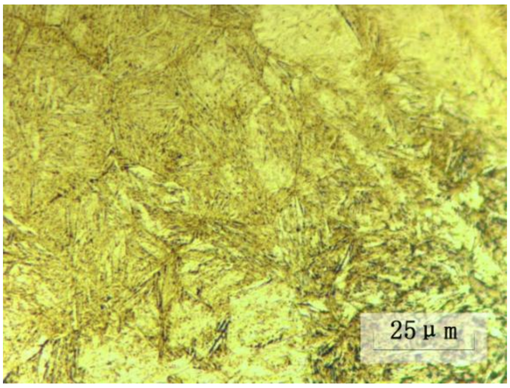

Figure 1. Microstructure of 23Co14Ni12Cr3Mo Steel

2.2. Slow strain rate tests

The specimens were cut into plate specimens in tensile direction, the shape of which was shown in Fig.2. The specimens were loaded by Letry SSRT Machine (WDML-5, China). The strain rate was set at 1×10^{-6}mm·min^{-1}. The specimens were exposed to Specific NaCl solution (1.5wt.%, 3.5wt.%, 5wt.%, 10wt.%). The specimens exposed to 3.5wt.% NaCl solution were applied with different potential. After tests, the fracture morphologies were characterized using scanning electron microscope (SEM3400, Britain).

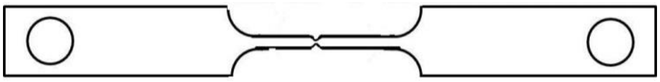

Figure 2. Schematic diagram of the specimen for the SSRT

2.3 Electrochemical measurements

The electrochemical measurements were performed using a conventional three-electrode electrochemical cell by an electrochemical system (Princeton2273, USA). A specimen with 1 cm^2 surface area, a platinum sheet and a saturated calomel electrode (SCE) served as the working electrode, the counter electrode and the reference electrode, respectively. The polarization curves were measured in 3.5wt.% NaCl solution at room temperature. The electrochemical impedance spectroscopy (EIS) tests were carried out different concentrations of NaCl solution(1.5wt.%, 5wt.% and 10wt.%) at room temperature. The frequency for electrochemical impedance spectroscopy (EIS) tests ranged from 1×10^5 Hz to 1×10^{-2} Hz. The impedance data was analyzed by Zsimpwin software.

3. RESULTS

3.1 Slow strain rate test results

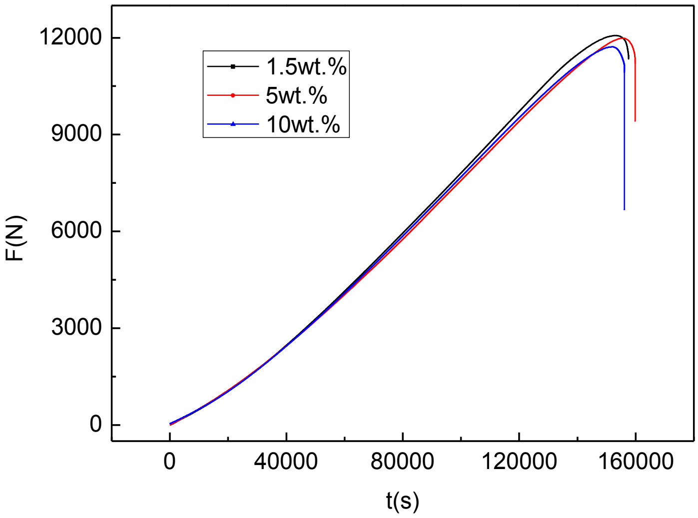

Figure 3. Axial force diagrams of 23Co14Ni12Cr3Mo steel under different NaCl concentration

The tensile force diagrams under the different NaCl concentrations are showed in Fig.3. With the positive shift of chloride ion concentration, it can be seen, the maximum tensile strength decreased. It has the biggest value as 12068N in 1.5wt.% NaCl concentration. With NaCl concentration increase from 1.5 to 5wt.%, the maximum tensile strength has a slight decrease, down to 11984N; while NaCl concentration increases from 5 to 10wt.%, the maximum tensile decrease to 11718N.

Fig. 4 presents the tensile force diagrams at different applied potential in 3.5wt.% NaCl solution. From Fig.5, it can be seen that, at the applied potential of -500mV, the maximum tensile strength has the biggest value as 11885N. For the applied potential lower than -500mV, with negative applied potential shift, the maximum tensile strength decreased. At the applied potential higher than -500mV, with the increase of applied potential, the maximum tensile strength decreased.

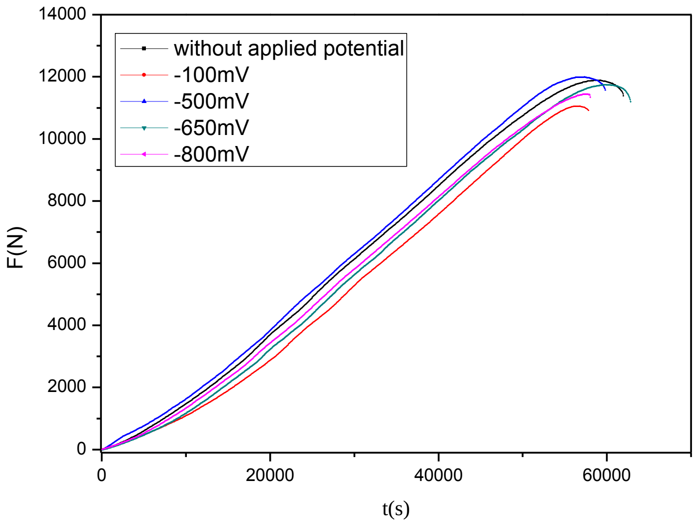

Figure 4. axial force diagrams of 23Co14Ni12Cr3Mo steel at different applied potential

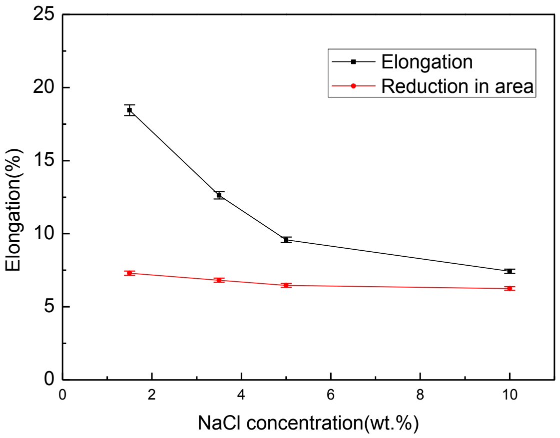

Figure 5. Elongations and reductions-in-area of 23Co14Ni12Cr3Mo under different NaCl concentrations

The elongations and reductions-in-area curves are presented in Fig.5. It can be seen with the increase of NaCl concentration, the elongation and reductions-in-area decrease. It has the biggest value as 18.44% and 7.29% separately at the 1.5wt.% NaCl concentration, the elongation in the seawater(3.5wt.%) control sample is 12.63% and the reduction-in-area is 6.82%. However, this is similar to the range of NaCl concentration from 5wt.% to 10wt.% with low elongations and reductions-in-area.

3.2 Fracture morphology after slow strain rate test

Fig.6 presents the SSRTs results comparing the fracture morphologies occurring in SSRTs conducted under different NaCl concentrations. The unprotected condition resulted in an obvious quasi-cleavage (QC), which shows it is controlled by the active dissolution reaction, and SSRTs revealed a trend towards brittle behavior. With the increase of Cl- ions, the fracture morphology tend to be smoother. In general, fractured surfaces occur as a result of stress corrosion cracking. As such, the mechanical and electrochemical characteristics of samples under the higher Cl^- concentration are poorer than that of samples under the lower concentration conditions.

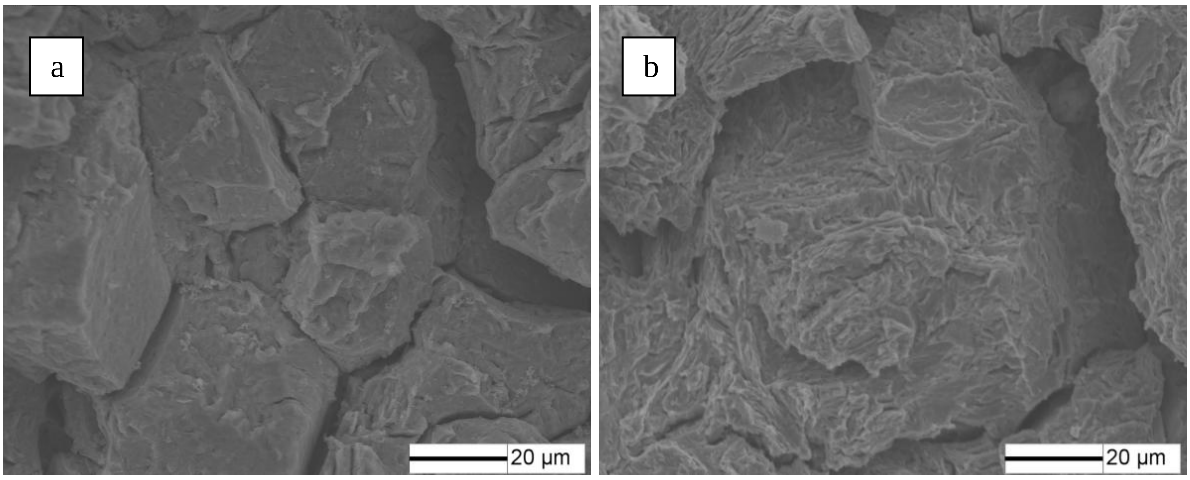

Figure 6. Surface morphologies of specimen after SSR tests under (a) 1.5wt.% (b) 10wt.% NaCl concentration

Figure 7 shows the comparison of the Sample fracture morphologies occurring in SSRTs conducted at various applied potentials. It can be seen that with a change in applied potentials, the fracture feature changes. At the applied potential of -100mV$_{SCE}$, Cleavage fracture was the dominant result and the fractured was evidence of the trend towards brittle behavior.

At the potential range between -500mV$_{SCE}$, the surface morphology showed a ductile fracture feature, with extensive distribution of dimples in the surface. Thus at the potential of -500mV$_{SCE}$, SSRTs revealed a trend towards gliding behavior, suggesting that there is a low SCC susceptibility.

For a potential range lower than -550mV$_{SCE}$, e.g.-650 and -800mV$_{SCE}$, the mixed fracture of ductile and brittle fracture behaviors were observed at the surface. With negative shift of applied potential at this potential range, brittle fracture is more obvious and bigger, which indicates the gliding fractures have a slight decrease. In general, fractured surfaces occurred as a result of stress corrosion cracking.

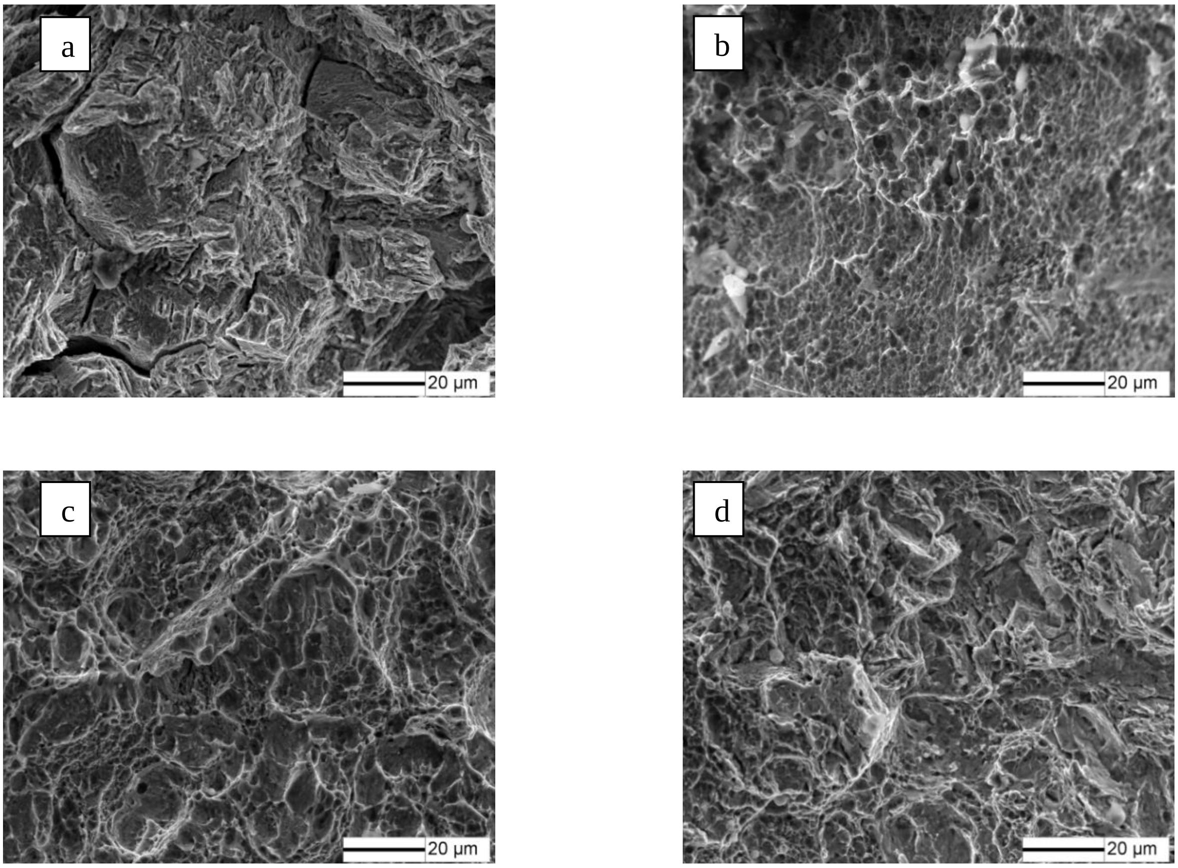

Figure 7. Surface morphologies of specimens after SSRT at (a)-100mV$_{SCE}$, (b)-500mV$_{SCE}$, (c)-650mV$_{SCE}$, (d)-800mV$_{SCE}$.

4. DISCUSSIONS

4.1 Effect of chloride concentration

4.1.1 Measurements of polarization curves

The Anodic and cathodic polarization curves for 23Co14Ni12Cr3Mo steel under different NaCl concentrations are showed in Fig.8. The E_{corr} and i_{corr} calculated from Fig.8 is listed in Table2. It is observed that the E_{corr} and i_{corr} have the biggest value as -453mV and 2.18×10^{-5} A·cm^{-2} separately at 1.5wt.% NaCl concentration. While E_{corr} and i_{corr} have the smallest value as -556mV and 3.77×10^{-5} A·cm^{-2}。

It can be seen that the E_{corr} decreased and the i_{corr} increased as the NaCl concentration increased from the Table2. This indicates that 23Co14Ni12Cr3Mo steel is more vulnerable to corrosion and the anodic dissolution rate increases with the increase of Cl^- ions, resulting in relatively flat fracture morphology and maximum tensile fracture to reduce.

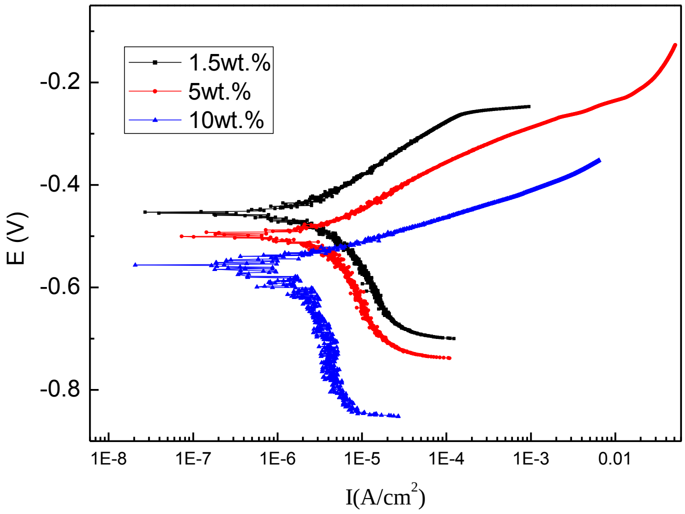

Figure 8. Anodic and cathodic polarization curves for 23Co14Ni12Cr3Mo steel under different NaCl concentrations

Table 2. The parameters of anodic and cathodic polarization curves for 23Co14Ni12Cr3Mo under different NaCl concentrations

NaCl concentration	E_{corr}/mV	$I_{corr}/A\cdot cm^{-2}$	R_a	R_c
1.5wt.%	-453	2.18×10^{-5}	0.104	-0.131
5 wt.%	-501	3.22×10^{-5}	0.084	-0.300
10 wt.%	-556	3.77×10^{-5}	0.048	-0.511

4.1.2 EIS simulation

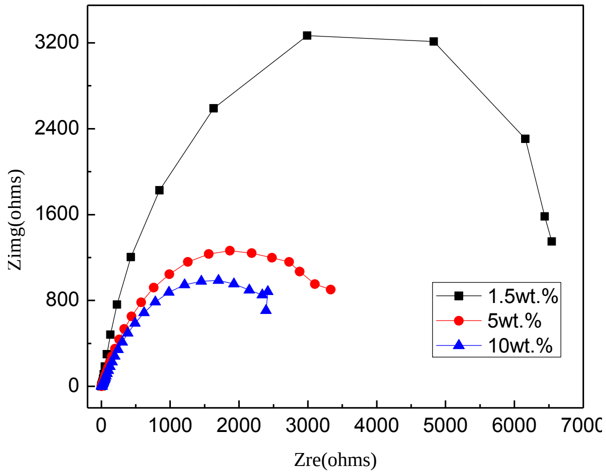

Figure 9. Nyquist diagrams of EIS measured under different NaCl concentrations

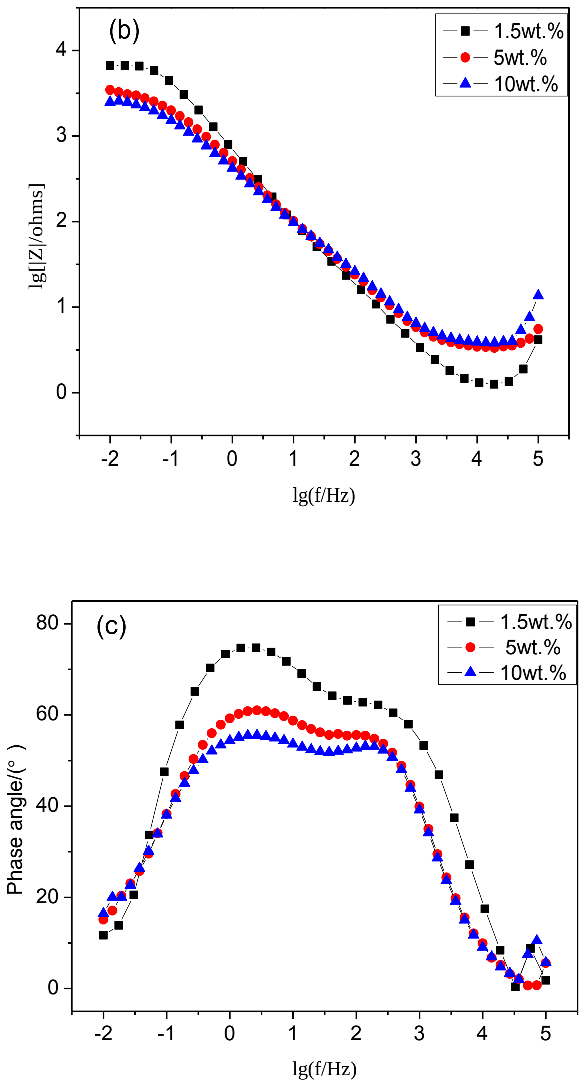

Figure 10. Bode diagrams of EIS measured under different NaCl concentrations: (a) impedance magnitude; (b) phase angle.

Fig.9 shows the EIS results in the form of Nyquist plots, in which the imaginary impedance (Z″) is plotted against the real impedance (Z′). From Fig.10, it is seen that the EIS responses of 23Co14Ni12Cr3Mo steel in various NaCl concentrations are featured with similar capacitance loop over the whole frequency range, but the impedance values are different from each other. The basic shapes of the capacitance loops are eccentric semicircles. It is obvious that the semicircle diameter shift with NaCl concentration increase from 1.5wt.% to 5wt.%, which is a typical indication that the corrosion rates of 23Co14Ni12Cr3Mo steel under different NaCl concentrations. This is in agreement with the previous polarization under different NaCl concentrations.

Fig.10 presents the Bode diagrams generated from the EIS data in Fig.9. From Fig.10(a), it is found that at different frequency range the impedance magnitudes has opposite trend with the increase of NaCl concentration. At the low frequency range from 10^{-2}Hz to 1Hz, the impedance magnitudes decrease as the increase of NaCl concentration, while at high frequency range from 10^{2}Hz to 10^{5}Hz, the impedance magnitudes decrease as the increase of NaCl concentration. The impedance magnitude at low frequency is related with the double-layer capacitance, while at high frequency, it is related with the solution resistance. From Fig.10(b), it is obvious that there is two time constants. It can deduce that a passive film forms on the specimen surface during the experimental process.

The electrochemical equivalent circuit of 23Co14Ni12Cr3Mo steel under different NaCl concentrations is presented in Fig.11, where R_s is the solution resistance, R_{ct} is related to the polarization resistance inversely proportional to the corrosion current density, R_{film} stands for the films resistance. Q_{dl} represents the CPE (constant phase angle element) used to replace the double-layer capacitance (C_{dl}) when the dispersion effect exists. Q is defined by $Q=Y_0(j\omega)^n$, where Y_0 is the admittance constant, n is the dispersion coefficient ($0\leq n\leq 1$). From Fig.11, The electrochemical reactions happen in the interface between passive film and substrate, Q_{film} represents the properties of passive film [14]. The impedance of the passive film can be expressed as[18]:

$$Z_{film}=\frac{R_{film}}{1+R_{film}Q_{film}(j\omega)^n}=\frac{R_{film}}{1+(j\tau\omega)^n} \qquad (1)$$

where τ is the relaxation time.

The corresponding electrochemical elements values simulated by electrical equivalent circuit in Fig.11 and τ values calculated by Eq.(1) are listed in Table3. It is seen that, the specimens have the highest film resistance R_{film} value as $7532\Omega\cdot cm^2$ under NaCl concentration of 1.5wt.%, and R_{film} decrease as the increase with NaCl concentration. As the NaCl concentration from 1.5wt.% to 5wt%, R_{film} values decreased significantly reduced to half. R_{ct} has the similar trend, but with smaller range ability. While the Q_{film}'s dimensions are related to the value n, it cannot be compared with each other. However with the increase of NaCl concentration, τ values have a significantly increase. This is consistent with the SSRT result before, indicating that τ values are closely related with the susceptibility to SCC of 23Co14Ni12Cr3Mo steel.[18]

The decrease of R_{film} and R_{ct} with the increase of Cl^- ions, suggest that the corrosion resistance decrease, resulting in the increase of i_{corr}. As demonstrated before, this leads to relatively flat fracture morphology and maximum tensile fracture to reduce.

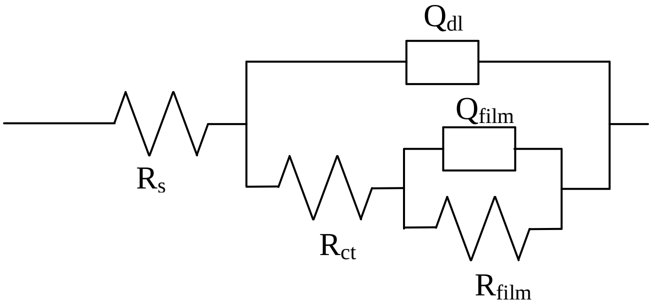

Figure 11. Electrochemical equivalent circuits of 23Co14Ni12Cr3Mo steel

Table 3. EIS data fitting results of 23Co14Ni12Cr3Mo steel under different NaCl concentrations

NaCl concentration	$R_s/\Omega\cdot cm^2$	Q_{dl} -$Y_0/\Omega^{-1}cm^{-2}\cdot s^{-n}$	Q_{dl} -n	R_{ct} $/\Omega\cdot cm^2$	Q_{film} -$Y_0/\Omega^{-1}cm^{-2}\cdot s^{-n}$	Q_{film} -n	R_{film} $/\Omega\cdot cm^2$	τ/s
1.5wt.%	1.178	1.733×10^{-4}	0.8569	58.87	$1.021\text{x}10^{-4}$	0.9128	7532	0.745
5wt.%	3.293	1.499×10^{-4}	0.846	54.47	$3.542\text{x}10^{-4}$	0.6936	3857	1.568
10wt.%	3.711	1.345×10^{-4}	0.8488	52.88	$5.274\text{x}10^{-4}$	0.6587	3182	2.195

4.2 Effect of applied potential

The effects of different scan rates on polarization are displayed in Fig.12.These polarization curves are generally similar, which indicates that the 23Co14Ni12Cr3Mo steel has similar electrochemical polarization behavior in 3.5wt.% NaCl solution. Results show that the SCC is attributed to the active dissolution at the cathodic polarization stage. At the low rate scan curve, the SCC is controlled by the active dissolution at the anodic polarization stage. For a scan rate range from 0.5 to 50mV/s, the range of the active dissolution reaction, the slow strain rate tests reveal a trend towards diffusion control behavior.

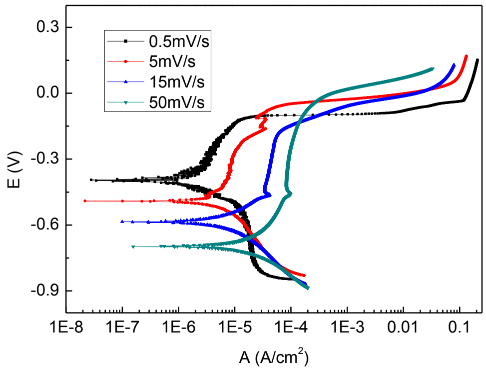

Figure 12. Effect of scanning rate on polarization curves of 23Co14Ni12Cr3Mo steel in 3.5wt.% NaCl solution

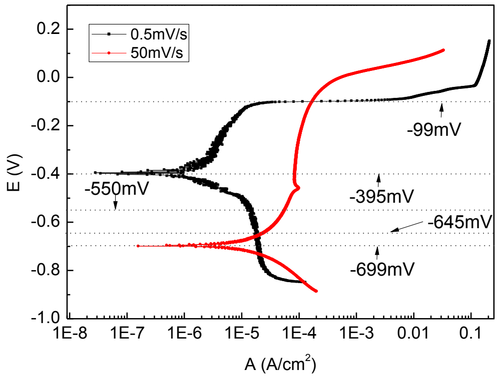

Figure 13. Fast and slow scanning rate polarization curves of 23Co14Ni12Cr3Mo steel in 3.5wt.% NaCl solution

During the slow scan rate testing with quasi steady state method, the electrode surface is sufficiently polarized, which can reflect the electrochemical characteristics of metal surface. The polarized scan rate is quick at the fast scan process, and no protective corrosion product film can be formed throughout the experiment to reflect the electrochemical characteristics of the fresh metal surface. It is supposed that the fast scan rate polarization curve can reflect the electrochemical characteristics of crack tip. So at the different electrode potentials, the SCC sensitivity can be represented by the differences between the fast scan rate current density (i_f) and the slow scan rate current density (i_s) [19~22]. It can be seen the corrosion potential(E_{corr}) of the fast scan rate curve is significantly lower than that of the slow scan rate curve in Fig.2, which shows the electrochemical activity of crack tip is much higher than the metal surface covered with corrosion production.

As mentioned before, the fast and slow scan rates tests simulate the crack tip and metal surface conditions, respectively. To show it clearly, the applied potentials were marked on polarization curves as can be seen in Fig.13. Four main regions can be seen on the polarization curves.

At first zone where potentials are more anodic than -395mV$_{SCE}$, both crack tip and metal surface were under anodic dissolution state, indicating that the SCC mechanism is anodic dissolution based. In the potentials range from -99 to -395mV$_{SCE}$, $i_f > i_s$, while the potentials is above -99mV$_{SCE}$, $i_f < i_s$. With positive shift of potential at first zone, i_f and i_s increase. This means that, with applying more anodic polarization, the SCC sensitivity increase. The fracture morphology at -100mV contain flat surface, showing sign of anodic dissolution.

At second zone,-645 to -395mV$_{SCE}$, the crack tip was under anodic dissolution state, while metal surface was under cathodic polarization. With the decrease of polarization potential at this zone, the current at fast scanning rate decrease, but current density at slow scanning rate increase. Thus, the oxidation rate of iron at crack tip decrease and the rate of reduction of hydrogen at metal surface increase. In the applied potentials range from -550 to -395mV$_{SCE}$, the current density at slow scanning rate is considerable small ($i_s < 10^{-5} A\cdot cm^{-2}$). While in the potentials range from -645 to -550mV$_{SCE}$, the slow scanning current density is relatively big. This indicates that, with applying more cathodic polarization at -645 to -550mV$_{SCE}$, the contribution of hydrogen embrittlement increases with respect to anodic dissolution.

At third zone, -699 to -645mV$_{SCE}$. The current density change trend with the decrease of polarization potential is the same as second zone. But, compared to the current density of slow scanning rate, fast scanning rate current density is very small, results in dominance of hydrogen embrittlement, and anodic dissolution accelerates the cracking process.

At zone IV where potentials are lower than -699mV$_{SCE}$, both crack tip and metal surface were in cathodic polarization mode. As applied potential increased more cathodically, the rate of reduction of hydrogen at crack tip and metal surface increase, which indicating that there is an increment in SCC susceptibility.

4. CONCLUSIONS

The effect of applied potential and chloride concentration on the stress corrosion cracking behavior of 23Co14Ni12Cr3Mo ultra-High strength steel were investigated.

From the characterization results, we can get the conclusions as following:

1) Both chloride ions and applied potential can obviously affect the corrosion behavior of the material: with the increase of NaCl concentration from 1.5 to 10wt.%, the ultimate tensile strength and plasticity decrease remarkably from 12068N to 11718N; at the applied potential of -500mV, the maximum tensile strength has the biggest value as 11885N, both negative and positive potential shift decrease the maximum tensile strength, the maximum tensile strength at -800mV is 11445N, and it is 11052N at -100mV.

2) The fracture morphologies after SSRTs in NaCl solution without applied potential shows as obvious quasi-cleavage. At the potential range between -500mV$_{SCE}$, the surface morphology showed a ductile fracture feature; with negative or positive shift of applied potential, SSRTs revealed a trend towards brittle behavior.

3) With the increase of NaCl concentration from 1.5 to 10wt.%, the E_{corr} decreased from -453mV to -556mV, the R_{film} decreased from 7532 to 3182Ω·cm^2, while the i_{corr} increased from 2.18×10^{-5} to 3.77×10^{-5}A·cm^{-2}.

4) Fast and slow scanning rate polarization is a promising tool for predicting material stress corrosion cracking mechanisms. The SCC of 23Co14Ni12Cr3Mo steel is attributed to the active dissolution, combined with hydrogen induced cracking.

ACKNOWLEDGEMENT
This work was supported by the National Science Foundation of China (51171011).

References

1. Y.B. Hu, C.F. Dong, M. Sun, K. Xiao, P. Zhong, X.G. Li. *Corros. Sci*. 53(2011)4159.
2. D Figueroa, Robinson. *Corros Sci*. 52(2010)1593.
3. R.L. Thomas, J.R. Scully, R.P. Gangloff. *Metall. Mater. Trans. A.* 34(2003) 327.
4. H.S. Costa-Mattos, I.N. Bastos, J.A. Gomes. *Corros. Sci*. 50(2008)2858.
5. A. Ashur, I. E. Klein, J. Sharon. *Mater. Des.* 16(1995)195.
6. E.I. Meletis. *J. Mech. Behav. Mater.* 7(2011)1.
7. G. Swati, C. Rana, S. Preet, V. Kain, M. Vivek. *Mater. Des.* 32(2011) 3823.
8. S. M. Haleem, E.I. Abd, A. WaneesS, A. E. AalE, A. Diab. *Corros. Sci*.52(2010)292.
9. B. Huet, V.L. Hostis, L. Tricheux, H. Idrissi. *Mater. Corros*. 61(2010)111.
10. R. K. Singh Raman. *Mater. Sci. Eng., A* . 441(2006)342.
11. K. L. Ma, Y.J. Xie, C.L. Guang, K.G. Wu. *J. Cent. South Univ.*17(2010)263.
12. A. Ashur, I.E. Klein, J. Sharon. *Mater. Des*. 16(1995)195.
13. M. Sun, K. Xiao, C.F. Dong, X.G. Li, P. Zhong. *J. Mater. Perform. Eng.*22(2012)1059.
14. J. Y. Zhong, M. Sun, D.B. Liu, X.G. Li, T.Q. Liu. *Int. J. Min. Met. Mat.* 17(2010)282.
15. J. H. Liu, C. Wen, M. Yu, S. M. Li, B. Wang. *Int. J. Electrochem. Sci.* 8 (2013) 4085.
16. J. H. Liu, S. Tian, S.M. Li, M. Yu. *Acta Aeronau et Astron Sinica.* 32(2011)1164.
17. L. F. Wu, S.M. Li, J.H. Liu, M. Yu. *J. Cent. South Univ.* 19(2012)2726.
18. J. S. Baek, J.G. Kim, D.H. Hur, J. S. Kim, *Corros. Sci*. 45(2003)983.
19. R. N. Parkins. *Corros. Sci*. 20(1980)147.
20. Z.Y. Liu, X.G. Li, Y.R. Zhang, C.W. Du, G.L. Zhai. *Acta Metall. Sin. (Engl. Lett.)* 22(2009)58.
21. Z.Y. Liu, X.G. Li, C.W. Du, G.L. Zhai, Y.F. Cheng. *Corros. Sci*. 50(2008)2251.

22. M. Javidi, S. Bahalaou Horeh. *Corros. Sci*. 80(2014)213.